Water Mass Transformations in the Southern Ocean Diagnosed from Observations: Contrasting Effects of Air–Sea Fluxes and Diapycnal Mixing

GUALTIERO BADIN*

Institute of Oceanography, University of Hamburg, Hamburg, Germany

RICHARD G. WILLIAMS

School of Environmental Sciences, University of Liverpool, Liverpool, United Kingdom

ZHAO JING AND LIXIN WU

Physical Oceanography Laboratory, Ocean University of China, Qingdao, China

(Manuscript received 7 November 2012, in final form 13 March 2013)

ABSTRACT

Transformation and formation rates of water masses in the Southern Ocean are estimated in a neutral-surface framework using air–sea fluxes of heat and freshwater together with in situ estimates of diapycnal mixing. The air–sea fluxes are taken from two different climatologies and a reanalysis dataset, while the diapycnal mixing is estimated from a mixing parameterization applied to five years of Argo float data. Air–sea fluxes lead to a large transformation directed toward lighter waters, typically from -45 to -63 Sv (1 Sv $\equiv$ 10^6 m^3 s^{-1}) centered at $\gamma = 27.2$, while interior diapycnal mixing leads to two weaker peaks in transformation, directed toward denser waters, 8 Sv centered at $\gamma = 27.8$, and directed toward lighter waters, -16 Sv centered at $\gamma = 28.3$. Hence, air–sea fluxes and interior diapycnal mixing are important in transforming different water masses within the Southern Ocean. The transformation of dense to lighter waters by diapycnal mixing within the Southern Ocean is slightly larger, though comparable in magnitude, to the transformation of lighter to dense waters by air–sea fluxes in the North Atlantic. However, there are significant uncertainties in the authors' estimates with errors of at least ± 5 W m^{-2} in air–sea fluxes, a factor 4 uncertainty in diapycnal mixing and limited coverage of air–sea fluxes in the high latitudes and Argo data in the Pacific. These water mass transformations partly relate to the circulation in density space: air–sea fluxes provide a general lightening along the core of the Antarctic Circumpolar Current and diapycnal diffusivity is enhanced at middepths along the current.

1. Introduction

The overturning circulation in the Southern Ocean is primarily controlled by a combination of surface buoyancy forcing and diapycnal mixing, but the relative importance of each process for different water masses is unclear. The meridional transfer across the Antarctic Circumpolar Current (ACC) is achieved via an upper overturning cell involves a formation and subduction of Subantarctic Mode Water (SAMW) and Antarctic Intermediate Water (AAIW) and a deep cell involving the formation of Antarctic Bottom Water (AABW) (presented in terms of a zonally averaged view in Fig. 1a). The northward transport within the surface and bottom cells is balanced by a southward return transport of deep waters, involving both Upper and Lower Circumpolar Deep Waters (UCDW, LCDW) and North Atlantic Deep Waters (NADW). The upper overturning cell is generally viewed as being controlled by a combination of winds and surface buoyancy fluxes, partly facilitated by mesoscale eddies transferring properties adiabatically in the ocean interior (Marshall 1997; Marshall and Radko 2006; Marshall and Speer 2012). While the deep overturning cell is viewed as involving dense bottom waters formed over the Antarctic shelves and subsequently modified by diapycnal mixing, enhanced over regions

* Additional affiliation: Program in Atmospheric and Oceanic Sciences, Princeton University, Princeton, New Jersey.

Corresponding author address: Gualtiero Badin, Institute of Oceanography, University of Hamburg, Bundesstrasse 53, D-20146 Hamburg, Germany.
E-mail: gualtiero.badin@zmaw.de

DOI: 10.1175/JPO-D-12-0216.1

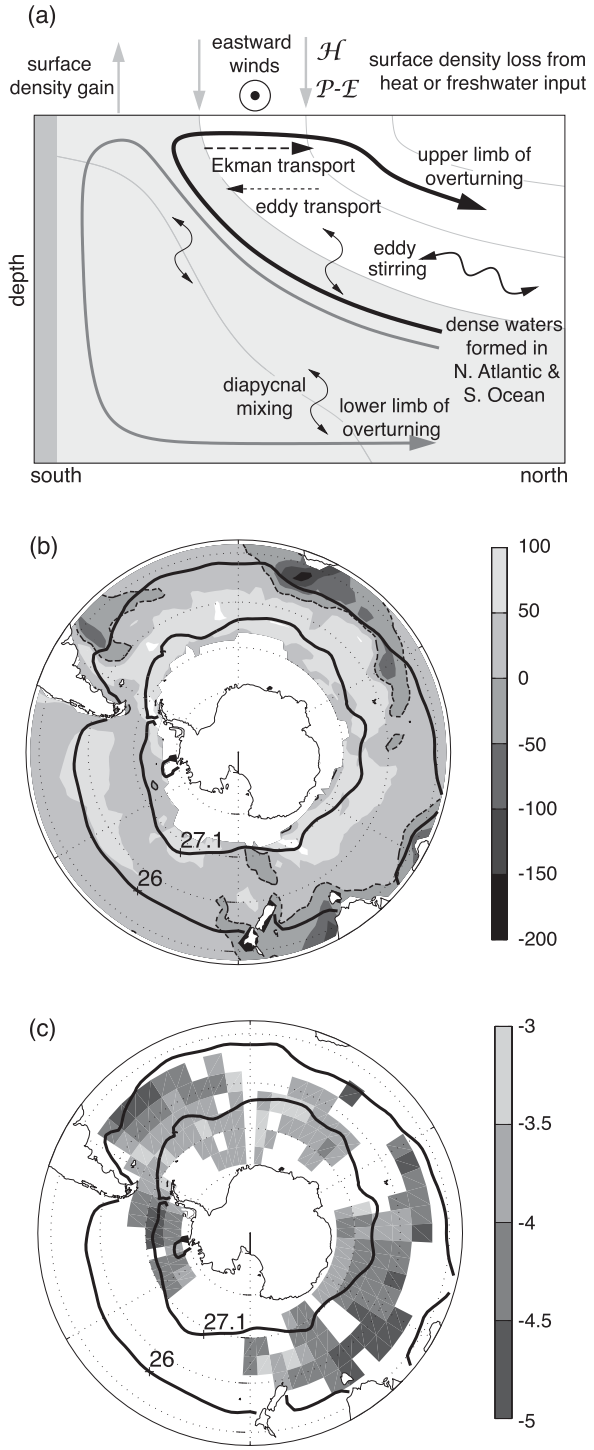

FIG. 1. (a) Schematic zonally averaged view of the Southern Ocean with two meridional overturning cells [redrawn from Williams and Follows (2011)], a northward transport of intermediate and bottom waters together with a southward transport of denser waters. (b) Total (heat + freshwater) equivalent heat flux into the ocean $\mathcal{H}^*$ ($\mathrm{W\,m^{-2}}$) from the WHOI climatology with a zero flux line (thin dashed line). (c) Vertical diffusivity ($\log_{10}K_z$; $\mathrm{m^2\,s^{-1}}$) from the Argo floats for 2005–10. Thick black lines indicate annual mean outcrops of $\sigma = 26$ and 27.1 surfaces from the *World Ocean Atlas 2009*.

of rough topography (Heywood et al. 2002; Naveira-Garabato et al. 2004; Wu et al. 2011), and transferred by upwelling and eddy stirring over the water column (Ito and Marshall 2008).

To compare the effects of air–sea fluxes and diapycnal mixing in the Southern Ocean, we apply a framework developed by Walin (1982) to understand the transformation of water masses. Transformation rates are diagnosed in neutral density coordinates γ (McDougall 1987a; Jackett and McDougall 1997); this choice avoids some problems in using potential density and errors from cabbeling and thermobaracity (McDougall 1987b), though there may still be additional transformation from the nonlinearities in the equation of state (Klocker and McDougall 2010). To understand the framework, consider a volume of fluid ΔV, bound by neutral density surfaces, γ and $\gamma + \Delta\gamma$, with an upper boundary given by the sea surface and an open boundary connecting to the rest of the ocean interior. The diapycnal volume flux or transformation G is defined as

$$G(\gamma) = \frac{1}{\Delta\gamma}\int_{\text{outcrop}} \mathcal{D}_{\text{in}}\, dA - \frac{\partial D_{\text{diff}}}{\partial\gamma}, \tag{1}$$

where $D_{\text{diff}} = -K(\partial\gamma/\partial z)$ is the diffusive density flux, and $\mathcal{D}_{\text{in}} = -(\alpha/C_p)\mathcal{H} + \beta\rho_0 S(\mathcal{E} - \mathcal{P})$ is the surface density flux into the ocean with the surface heat flux $\mathcal{H}(x, y)$ positive when directed into the ocean, and $\mathcal{E}(x, y)$ and $\mathcal{P}(x, y)$ are, respectively, the evaporation and precipitation rates; $C_p(T, S)$ is the heat capacity for seawater at constant pressure, $\alpha(T, S)$ and $\beta(T, S)$ are, respectively, the temperature T and salinity S dependent thermal expansion and the haline contraction coefficients of seawater, and $\rho_0 = 1027\,\mathrm{kg\,m^{-3}}$ is a reference density. A diapycnal volume flux directed from light to dense water $G(\gamma) > 0$ requires an increase in density either from the surface input of density arising from air–sea heat and freshwater fluxes $\int_{\text{outcrop}}\mathcal{D}_{\text{in}}\, dA > 0$ or from a convergence of diffusive density fluxes $-\partial D_{\text{diff}}/\partial\gamma > 0$. The rate of formation of water mass $M(\gamma)$ in the neutral density interval $\Delta\gamma$ is defined by the convergence of diapycnal volume fluxes $G(\gamma)$,

$$M(\gamma)\Delta\gamma = -\Delta\gamma\frac{\partial G}{\partial\gamma}. \tag{2}$$

The Walin framework has previously been applied to the Southern Ocean in inverse model studies (Speer et al. 2000; Sloyan and Rintoul 2001; Zika et al. 2009) and in a semi-analytical model (Badin and Williams 2010), where air–sea fluxes were controlled by the meridional deviation of surface isotherms induced by surface Ekman and eddy flows. Most applications of the

Walin framework have not employed independent estimates of diapycnal mixing and have instead diagnosed their contribution as a residual from the total transformation minus that provided by air–sea fluxes (Marsh et al. 2000; Downes et al. 2011). However, there are several exceptions, where the contribution to water mass transformation from diapycnal mixing is directly diagnosed in numerical models (Nurser et al. 1999; Marshall et al. 1999; Iudicone et al. 2008); in particular, Nurser et al. (1999) found that most of the transformation from diapycnal mixing in the North Atlantic is confined to the tropics, where there are strong vertical density gradients within upwelling zones. In a different dynamical regime, the European shelf-break front, Badin et al. (2010) found that air–sea fluxes and diapycnal mixing are of comparable importance in determining the transformation but act on different density classes and do not compensate locally.

In this study, the relative contributions from air–sea fluxes and diapycnal mixing to the transformation and formation rates in the Southern Ocean are estimated making use of three datasets for surface fluxes and mixing estimates diagnosed from Argo float data, including diagnostics for the separate sectors of the Southern Ocean. The transformations in the Southern Ocean are finally discussed in terms of the connection with the air–sea transformation rates in the North Atlantic and how the air–sea fluxes and diapycnal mixing link to the path of the Antarctic Circumpolar Current.

2. Datasets for air–sea fluxes and diapycnal mixing

a. Air–sea fluxes

Surface density fluxes over the Southern Ocean are estimated south of 30°S using three different datasets: the Woods Hole Oceanographic Institution (WHOI) objectively analyzed air–sea fluxes (OAFlux) project (Yu et al. 2008) with a 1° resolution from 2005 to 2009; the 2.0 National Oceanography Centre, Southampton (NOC) air–sea fluxes climatology (Berry and Kent 2011) with a 1° resolution covering from 2005 to 2010; and the National Centers for Environmental Prediction (NCEP)–National Center for Atmospheric Research (NCAR) weather center reanalysis (Kalnay et al. 1998) with a 2° resolution including 2005–10; for an analysis of their differences, see Cerovecki et al. (2011). The evaporation rate is diagnosed from the latent heat fluxes, the NCEP–NCAR weather center reanalysis data for precipitation is used for each dataset, and the ocean temperature and salinity fields are taken from the *World Ocean Atlas 2009* (Locarnini et al. 2010; Antonov et al. 2010) with 1° resolution.

The heat and freshwater fluxes are expressed here as an equivalent heat flux

$$\mathcal{H}^* = \mathcal{H} - \frac{\beta \rho_0 S C_p}{\alpha}(\mathcal{E} - \mathcal{P}), \tag{3}$$

where positive values represent a lightening from surface heat gain or freshwater input. The averaged fluxes over the 2005–09 period from the WHOI climatology reveal extensive regions of surface lightening, $\mathcal{H}^* \approx 100\,\mathrm{W\,m^{-2}}$, away from the land in the Atlantic–Indian and eastern Pacific sectors of the Southern Ocean. In contrast, there is stronger surface cooling $\mathcal{H}^* \approx -200\,\mathrm{W\,m^{-2}}$ and an increase in surface density, where the air passes from over the land to over warm ocean boundary currents, such as the Agulhas Current off South Africa, in the Argentine Basin, and off the Australia coast (Fig. 1b).

b. Mixing data

The diapycnal mixing is estimated via finescale strain measurements provided by 5337 Argo floats over the Southern Ocean (from 40° to 75°S) with a maximum depth of 1800 m and from 2005 to 2010 (Wu et al. 2011). The depth range is sufficient to resolve the transformation of intermediate and some deep waters, while the transformation of denser bottom water, AABW, is resolved only along the Antarctic shelf.

FINESCALE STRAIN CLOSURE FOR VERTICAL DIFFUSIVITY

To calculate the vertical diffusivity, the profiles are separated into 300-dbar segments, each partly overlapping; segments with an upper bound shallower than 300 dbar are discarded because of the presence of sharp pycnoclines. The vertical diffusivity is evaluated using a finescale strain closure (Gregg et al. 2003; Kunze et al. 2006)

$$K_z = K_0 \frac{\langle \zeta_z^2 \rangle^2}{\langle \zeta_z^2 \rangle_{\mathrm{GM}}^2} h_2(R_\omega) J\left(\frac{f}{N}\right), \tag{4}$$

where $\langle \zeta_z^2 \rangle^2$ is the observed strain variance, $\langle \zeta_z^2 \rangle_{\mathrm{GM}}^2$ is the strain variance from the Garrett–Munk (GM) model spectrum, h_2 is a function of the shear/strain variance ratio R_ω, and $J(f/N)$ is a latitude-dependent function of the Coriolis parameter f and buoyancy frequency N. The internal wave strain is estimated from depth contrasts in the buoyancy frequency $\zeta_z = [N^2(z) - \overline{N}^2]/\overline{N}^2$, depending on $N^2(z)$ varying with depth and $\overline{N}^2$ based on quadratic fits to each profile segment (Polzin et al. 1995). The strain variance is determined as

$$\langle \zeta_z^2 \rangle^2 = \int_{k_1}^{k_2} \phi(k)\, dk = 0.1, \tag{5}$$

where $\phi(k)$ is the spectral representation, k_1 and k_2 are the minimum and maximum vertical wavenumbers, respectively; the choice of the constant, 0.1, on the right-hand side is rather arbitrary, although changes in its value only have a minor effect on the diagnosed mixing. The GM strain variance is computed over the same wavenumber band. The dissipation rate is related to the vertical diffusivity by

$$\epsilon = K_z \frac{N^2}{\Gamma}, \tag{6}$$

where Γ is the mixing efficiency, typically taken to be 0.2 (Osborn 1980). The shear/strain ratio R_ω is set to 7 following Kunze et al. (2006). As the finescale parameterization is only able to reproduce microstructure diffusivities to within a factor of 2, using strain only with a fixed value of R_ω leads to uncertainties in vertical diffusivity of a factor of 4. Potential contamination in segments with strong changes in stratification is avoided by applying a test identifying and discarding problematic segments (Kunze et al. 2006). The diffusivity estimates are binned in the horizontal with a resolution of 6° in longitude and a 7° in latitude; however, even with this large horizontal binning, large sectors of the Southern Ocean are under sampled, especially over the Pacific sector.

The resulting vertically integrated estimates of vertical diffusivity have a patchy distribution affected by the large bins (Fig. 1c), with larger values possibly along the annual-averaged outcrop of $\gamma = 27.1$, on the poleward flank of the ACC. Using this dataset, Wu et al. (2011) found that high values of vertical diffusivity between 1200 and 1800 m are positively correlated with regions of rough topography. Similarly, in a global analysis of the diapycnal mixing implied from Argo data, Whalen et al. (2012) found enhanced vertical diffusivity in regions of rough topography and eddy kinetic energy, as well as enhanced values in regions of low stratification at high latitudes.

3. Transformation and formation rates from air–sea fluxes and diapycnal mixing

The transformation and formation rates are now separately estimated for the air–sea fluxes and diapycnal mixing over the Southern Ocean and its separate sectors, emphasizing first the new estimates from diapycnal mixing.

a. Transformation rates from interior diapycnal mixing

The density fluxes from diapycnal mixing are diagnosed over the neutral density range $26.7 \le \gamma \le 28.45$ using an interval of $\Delta\gamma = 0.1$. The vertical diffusivity averaged along neutral density surfaces generally increases for denser waters (Fig. 2a, full line). The resulting transformation is either directed to denser waters, reaching 7.6 Sv ($1\,\text{Sv} \equiv 10^6\,\text{m}^3\,\text{s}^{-1}$) centered at $\gamma = 27.8$ or conversely directed to lighter waters reaching −16.3 Sv centered at $\gamma = 28.3$ (Fig. 2b, full line).

The resulting water mass formation from the convergence of the transformation rates reaches a maximum of 7.9 Sv at $\gamma = 28.1$ (Fig. 2c, full line). The transformation rate estimates are affected by large uncertainties arising from the factor of 4 in the uncertainty in diapycnal diffusivity and the under sampling of regions of the Southern Ocean (Fig. 1c).

To account for the large regions of missing data, a second estimate of the transformation rates from interior mixing is provided by extrapolating the neutral density–averaged values of the vertical diffusivity (based on the restricted coverage in Fig. 1c) to apply to the spatially varying neutral density over the entire Southern Ocean (taken from the *World Ocean Atlas 2009*). The resulting transformation is increased in magnitude as expected given the greater assumed area coverage: a larger transformation directed to dense waters of 24.3 Sv at $\gamma = 27.8$ and directed to lighter waters of −53.3 Sv at $\gamma = 28.3$ (Fig. 2b, dashed line). The implied water mass formation over the entire Southern Ocean then increases to a maximum of 32.6 Sv at $\gamma = 28.2$ (Fig. 2c, full line). However, these estimates of water mass transformation and formation should be viewed as likely upper bounds, as this extrapolation probably includes an incorrect attribution of vertical diffusivity to regions where Argo data are not available. Henceforth, we prefer to focus on the transformation rates estimated from interior mixing evaluated only where Argo data are available.

b. Equivalent heat fluxes

Surface density fluxes, and corresponding equivalent heat fluxes (3), are collected into monthly means based upon area averaging of air–sea fluxes between density outcrops for each month. Annual fluxes are evaluated using these area-weighted surface fluxes for each month with a neutral density range $26 \le \gamma \le 27.6$ and an interval of $\Delta\gamma = 0.1$.

In all the datasets, the total equivalent heat flux is positive over the entire neutral density range (Figs. 3a–c, full line). In the WHOI climatology, the total equivalent heat flux reaches 50 W m^{-2} at $\gamma = 27.3$ (Fig. 3a, full line), achieved predominately by surface warming for light surfaces, $\gamma < 27.2$, and freshening for denser surfaces, $27.2 \le \gamma < 27.6$ (Fig. 3a, dashed and dot–dashed lines respectively). Similarly, in the NOC climatology and in

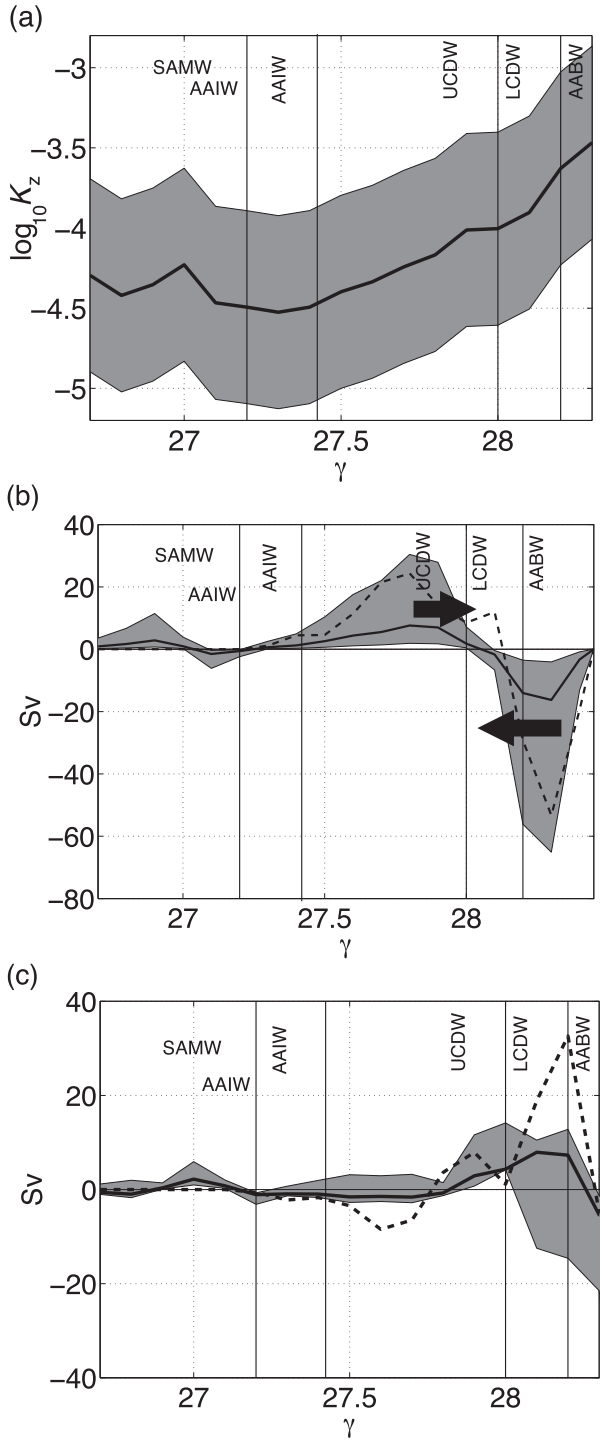

FIG. 2. (a) Vertical diffusivity ($\log_{10}K_z$; $m^2 s^{-1}$) from the Argo floats for the 2005–10 period averaged within neutral density with $\Delta\gamma = 0.1$ bins. (b) Transformation and (c) formation rates (Sv) from the diapycnal fluxes calculated over the points where Argo data are available (full line) and extrapolating over the entire Southern Ocean by assuming the vertical diffusivity averaged over neutral density from the Argo floats applies to the neutral density distribution over the entire Southern Ocean (dashed lines). The gray area represents the effect of a factor 4 change in K_z for the transformation and formation rates.

the NCEP reanalysis, the total equivalent heat flux reaches 46 W m^{-2} at $\gamma = 27.5$ and 50 W m^{-2} at $\gamma = 27.3$, with the surface warming dominating over the freshening for light surfaces, $\gamma < 26.9$ and $\gamma < 27.0$, respectively (Figs. 3b,c).

c. *Transformation rates from air–sea fluxes and diapycnal mixing*

The annual transformation rates are evaluated by summing the monthly transformations from air–sea fluxes for each outcrop during the 2005–10 period and combining with the annual transformation from the diapycnal mixing.

The transformation rate changes in sign across the surface density range spanning the Southern Ocean (Figs. 3d–f, full line). Based upon the WHOI climatology, with increasing density, the transformation is directed toward lighter waters, reaching −63 Sv at $\gamma = 27.2$, directed toward denser waters, reaching 8.1 Sv at $\gamma = 27.8$, and then directed toward lighter waters again, reaching −16.2 Sv at $\gamma = 28.3$ (Fig. 3d, full line). The transformation to lighter waters at $\gamma = 27.2$ corresponds to a conversion of intermediate waters to SAMW; see water mass definitions in Table 1 (Sloyan and Rintoul 2001; Hanawa and Talley 2001; Suga and Talley 1995). This transformation is achieved by surface warming and freshening along the equatorial flank of the ACC (Fig. 1b). At the same time, the densest and coldest part of the SAMW makes up the fresh layer of AAIW (McCartney 1977), which is then subducted, spreads northward, and becoming slightly denser, as revealed by low salinity and potential vorticity along $\gamma \sim 27.3$ (Suga and Talley 1995). For the denser waters, the diapycnal mixing dominates the transformation, converting intermediate waters to denser circumpolar waters at $\gamma = 27.8$ (Figs. 3d–f, dot–dashed line) and denser AABW to lighter circumpolar waters at $\gamma = 28.2$. In particular, the transformation by air–sea fluxes of SAMW and AAIW is much larger than the transformation by diapycnal mixing of AABW to LCDW.

Both the transformation rates diagnosed from NOC and NCEP–NCAR are similar in character to that from the WHOI climatology: the NOC climatology shows a weaker transformation to lighter waters of −45.1 Sv at $\gamma = 27.2$, while the NCEP–NCAR reanalysis reveals a transformation to lighter waters of −57.2 Sv in the same potential density class (Figs. 3e,f). The transformation provided by the air–sea fluxes (Fig. 3f, dashed line) is controlled by a comparable contribution from heat and freshwater fluxes in the neutral density range $26 \leq \gamma < 27$ and by the freshwater fluxes for denser waters, $\gamma > 27$ (Fig. 3f, dot–dashed line). Hence, there is a consistent picture with air–sea fluxes and interior

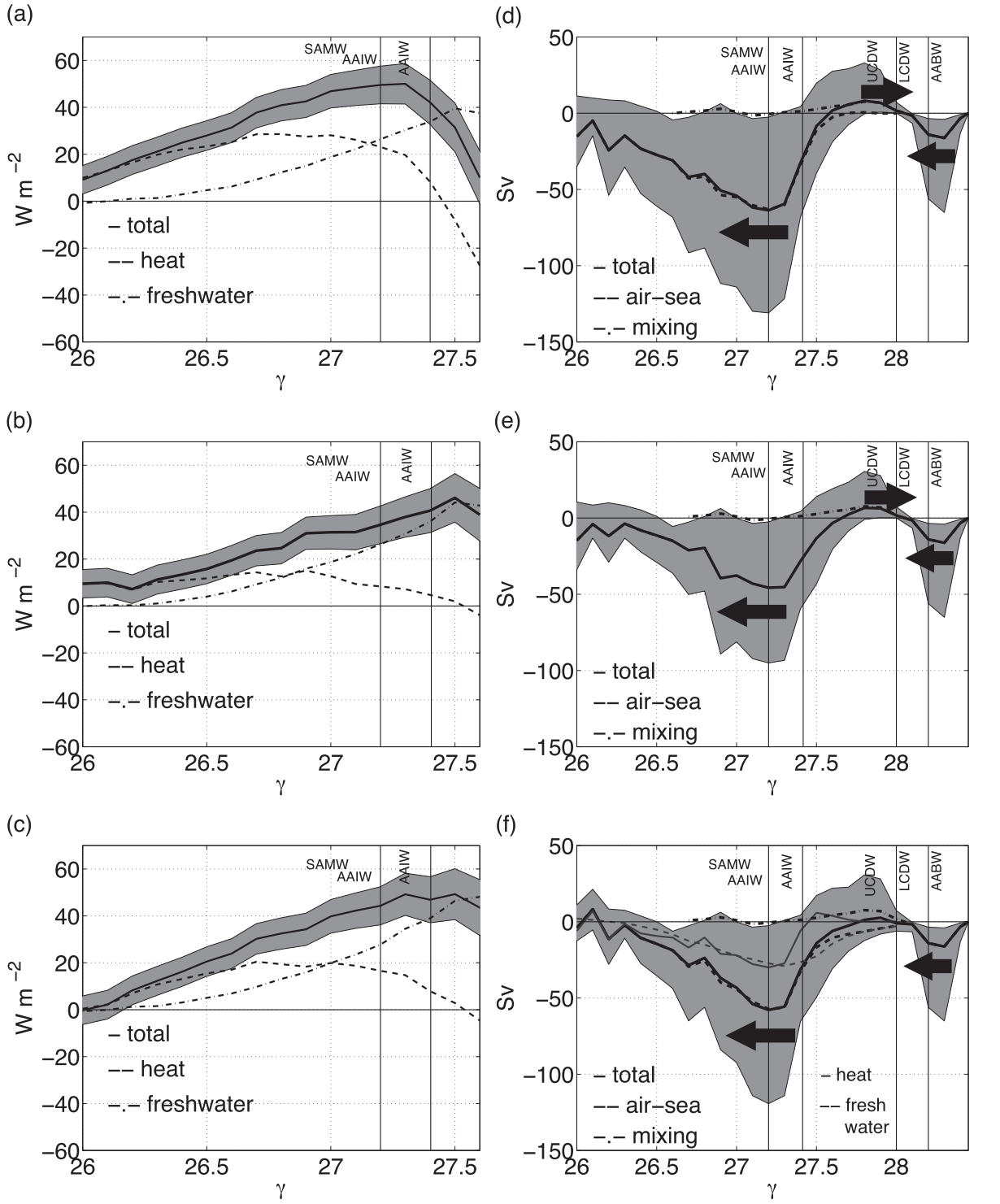

FIG. 3. (left) Air–sea fluxes (W m^{-2}) and (right) transformation (Sv) evaluated over the Southern Ocean using the (a),(d) WHOI, (b),(e) NOC climatologies, and (c),(f) NCEP–NCAR reanalysis. The air–sea fluxes are presented in terms of the total equivalent heat flux (full lines) using (3) from the heat (dashed line) and freshwater (dot–dashed line) components. The transformation rates are shown for the total (full line), the air–sea flux component (dashed line) and mixing component (dot–dashed line). The thin lines in (f) represent the separate contributions from the heat and freshwater components. The gray area represents the change in the total transformation from a ± 5 W m^{-2} change in the heat component of the density fluxes and a factor 4 variation in K_z.

TABLE 1. Definition of water masses in the Southern Ocean in neutral density, based upon a combination of Sloyan and Rintoul (2001), Hanawa and Talley (2001), and Suga and Talley (1995).

Water masses	γ
SAMW and newly formed AAIW	26.5–27.2
AAIW away from formation	27.2–27.4
UCDW	27.4–28.0
LCDW	28.0–28.2
AABW	28.2–bottom

diapycnal mixing acting on different neutral density classes and water masses.

d. *Formation rates from air–sea fluxes and diapycnal mixing*

The formation of water masses is calculated from the convergence of the transformation rates. Using the WHOI climatology, air–sea fluxes lead to a formation of SAMW and AAIW with a maximum rate of 7.7 Sv at γ = 26.65 and destruction at a maximum rate of −25.5 Sv at γ = 27.45 (Fig. 4a). Interior diapycnal mixing instead controls the formation of LCDW at a maximum rate of 16.3 Sv at γ = 28.3.

The formation rates of SAMW and AAIW diagnosed from NOC and NCEP–NCAR are broadly similar to that diagnosed from the WHOI climatology: the NOC climatology suggests a formation of SAMW and AAIW at a maximum rate of 9.8 Sv at γ = 26.95 and destruction at a maximum rate of −16 Sv at γ = 27.45, while the NCEP–NCAR reanalysis implies a formation of SAMW and AAIW at a maximum rate of 9.2 Sv at γ = 26.85 and destruction at a maximum rate of −20.8 Sv at γ = 27.45.

e. *Sector estimates of transformation and formation rates*

Given the spatial inhomogeneity of both the air–sea and the interior diapycnal fluxes, the transformation and formation rates for separate sectors of the Southern Ocean are calculated, where the Atlantic sector is from 70°W to 20°E, the Pacific sector from 130°E to 70°W, and the Indian sector from 20° to 130°E. The air–sea flux contribution to the transformation and formation rates is diagnosed from the WHOI climatology; estimates of water mass transformation and formation rates from the NOC climatology and the NCEP–NCAR reanalysis (not shown) show similar patterns, but differ in magnitude.

In the Atlantic sector, air–sea fluxes lead to a transformation toward lighter waters (Fig. 5a), reaching −18.8 Sv at γ = 27.1, corresponding to converting intermediate waters to lighter SAMW and AAIW. Diapycnal mixing leads to a transformation both directed

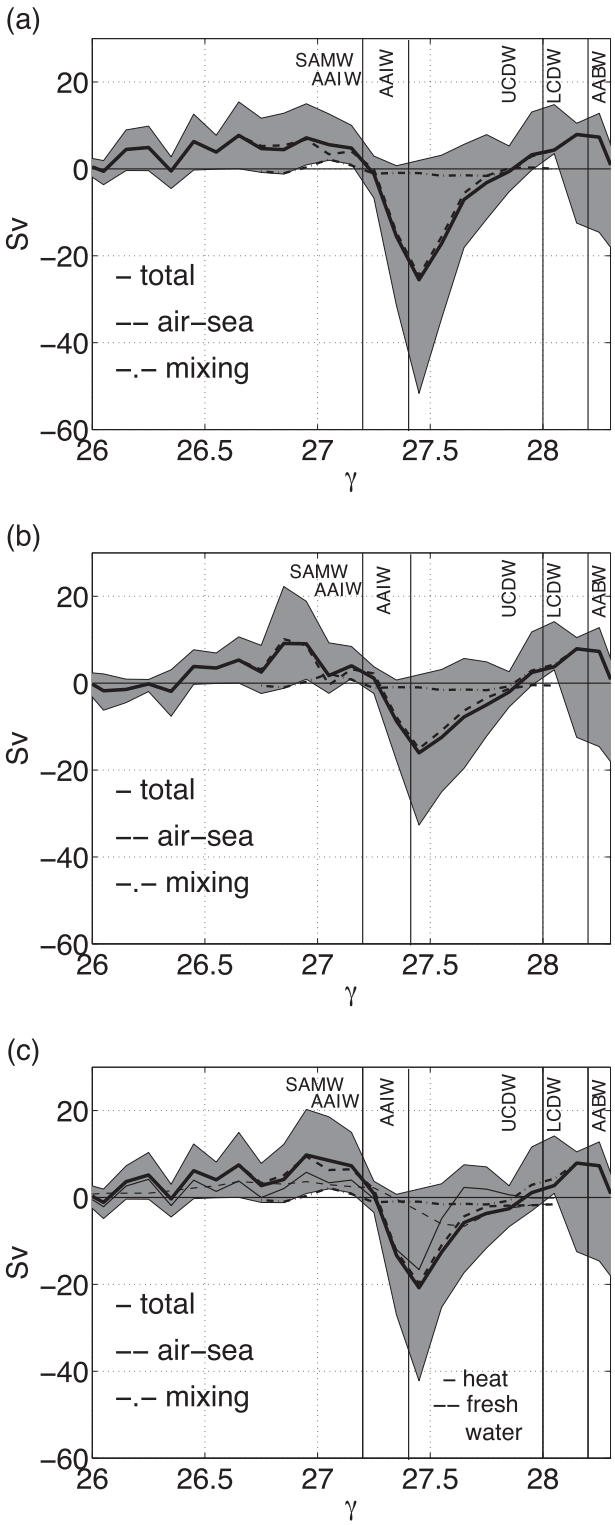

FIG. 4. Total formation rates (Sv) for the Southern Ocean from the (a) WHOI and (b) NOC climatologies and (c) NCEP–NCAR reanalysis: the total (full line), and the air–sea flux (dashed line) and mixing components (dot–dashed line). The thin lines in (c) represent the separate contributions from the heat and freshwater components; shading as in Fig. 3.

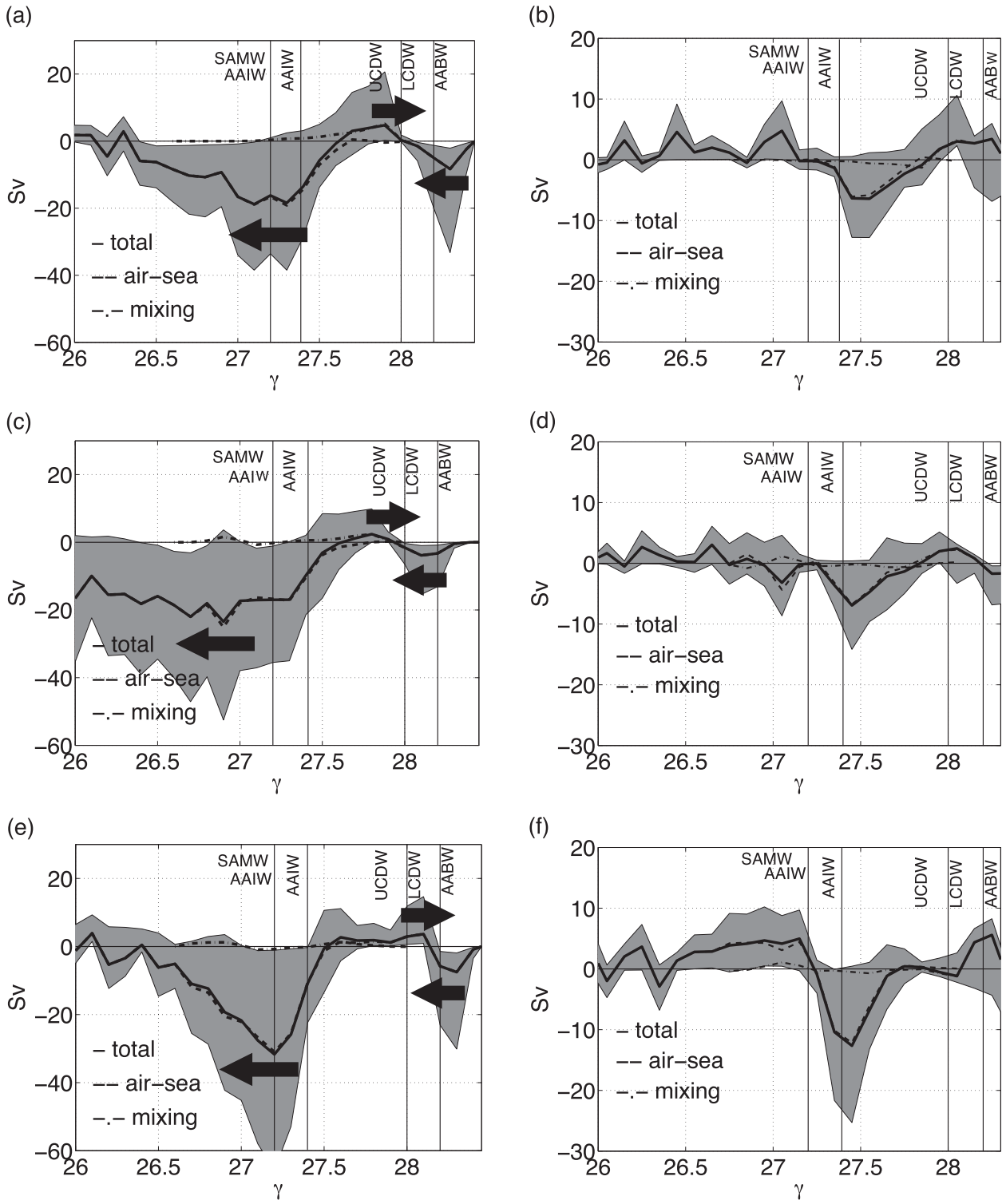

FIG. 5. (left) Transformation and (right) formation rates (Sv) for the (a),(b) Atlantic, (c),(d) Pacific, and (e),(f) Indian sectors of the Southern Ocean for the total (full line), and the air–sea flux (dashed line), and mixing components (dot–dashed line); shading as in Fig. 3.

toward denser waters, reaching 4.7 Sv at $\gamma = 27.9$, corresponding to a conversion to denser UCDW, and directed toward lighter waters, reaching −8.3 Sv at $\gamma = 28.3$, representing a conversion of AABW to lighter LCDW. Air–sea fluxes lead then to a formation of SAMW and AAIW, reaching 4.8 Sv at $\gamma = 27.05$, and a destruction of −6.4 Sv at $\gamma = 27.55$ (Fig. 5b), while diapycnal mixing leads to a formation of LCDW at a maximum rate of 3 Sv at $\gamma = 28.05$.

In the Pacific sector, air–sea fluxes again provides a transformation toward lighter waters (Fig. 5c), reaching −23.5 Sv at $\gamma = 26.9$, while diapycnal mixing leads to a transformation both toward denser waters, reaching 2.4 Sv at $\gamma = 27.8$, and toward lighter waters, reaching −3.9 Sv at $\gamma = 28.1$. Accordingly, air–sea fluxes imply a formation of SAMW and AAIW reaching 3 Sv at $\gamma = 26.65$ and a destruction reaching −6.9 Sv at $\gamma = 27.45$ (Fig. 5d). Diapycnal mixing also leads to a formation of LCDW reaching 3 Sv at $\gamma = 28.05$.

In the Indian sector, air–sea fluxes likewise drive a transformation toward lighter waters, reaching −31.7 Sv at $\gamma = 27.2$, and diapycnal mixing drives both a transformation toward denser waters, reaching 3.7 Sv at $\gamma = 28.1$, and toward lighter waters, reaching −7.5 Sv at $\gamma = 28.3$ (Fig. 5e). Consequently, air–sea fluxes lead to a formation of SAMW and AAIW, reaching 5 Sv at $\gamma = 27.15$, and a destruction reaching −12.6 Sv at $\gamma = 27.45$ (Fig. 5f). Diapycnal mixing implies a formation of LCDW reaching 5.6 Sv at $\gamma = 28.25$.

Thus, the three sectors show broadly similar patterns of transformation and formation of water masses.

f. Comparison with previous studies

Our transformation and formation diagnostics, based on air–sea fluxes from two different climatologies and a reanalysis dataset and diapycnal mixing diagnosed from Argo data, are in reasonable agreement with the analyses of hydrographic sections using a box model by Sloyan and Rintoul (2001, see their Fig. 13). There are similar patterns for the total transformation, though different magnitudes, to the ocean model study by Iudicone et al. (2008) and the coupled atmosphere–ocean model by Downes et al. (2011).

However, our observationally based diagnostics do not show a strong compensation between the air–sea flux and interior mixing components of the transformation rates, which are instead found in the modeling studies; this model compensation leads to a reduced transformation to SAMW and AABW. The difference between the observed and modeled transformation of AABW may be due to limitations of both the observational and modeling studies, since there is poor knowledge of air–sea mixing and direct estimates of mixing, as well as the models being particularly poor at representing the formation and spreading of bottom waters. In addition, these observational diagnostics emphasize a climatological state, which is probably inappropriate, as there might be large interannual variability in the transformation rates of mode waters, as illustrated by Cerovecki et al. (2013).

4. Discussion

The diagnostics for air–sea fluxes and diapycnal mixing are now discussed in terms of their possible connections with the transformation in the North Atlantic and the path of the Antarctic Circumpolar Current.

a. Dense-water transformation connection to the North Atlantic

The surface outcrops of $\gamma = 28.2$ over the global ocean suggest that these dense waters are formed and spread either from the North Atlantic or the Southern Ocean. To address this connection, the transformation from air–sea fluxes is estimated over the North Atlantic Ocean (22°–79°N and 120°W–0°) and compared with the total transformations estimated over the Southern Ocean for the 2005–10 period. Since the algorithm employed to calculate neutral density extends only up to 64°N (Jackett and McDougall 1997), the transformation rates are also diagnosed up to 79°N using potential density referred to the sea surface σ_0 (Fig. 6, thin full lines). The diagnosed transformation rates from each coordinate system are broadly similar, although the diagnostic using σ_0 reveals slightly less transformation within the most dense classes.

Over the North Atlantic, there is a similar picture for all three climatologies with light waters transformed to denser waters with a peak at $\gamma = 27.4$ (Fig. 6, thick full lines): the WHOI and NOC climatology suggests that the transformation reaches 12 Sv, while the NCEP–NCAR reanalysis suggests the transformation reaches 17 Sv. The transformation in the North Atlantic is always dominated by the contribution from the surface heat flux, rather than the freshwater fluxes (Fig. 6, dot-dashed lines).

These transformation rates from the air–sea fluxes over the North Atlantic for $\gamma > 27.3$ are smaller, though comparable in magnitude, to the transformation of dense waters to the lighter waters over the Southern Ocean of typically −16 Sv at $\gamma = 28.2$ (Figs. 3d–f, full line). Hence, the transformation of dense waters in the Southern Ocean induced by diapycnal mixing plausibly connects to the transformation of lighter to denser waters in the North Atlantic achieved by air–sea fluxes. There is also probably an augmentation of the formation

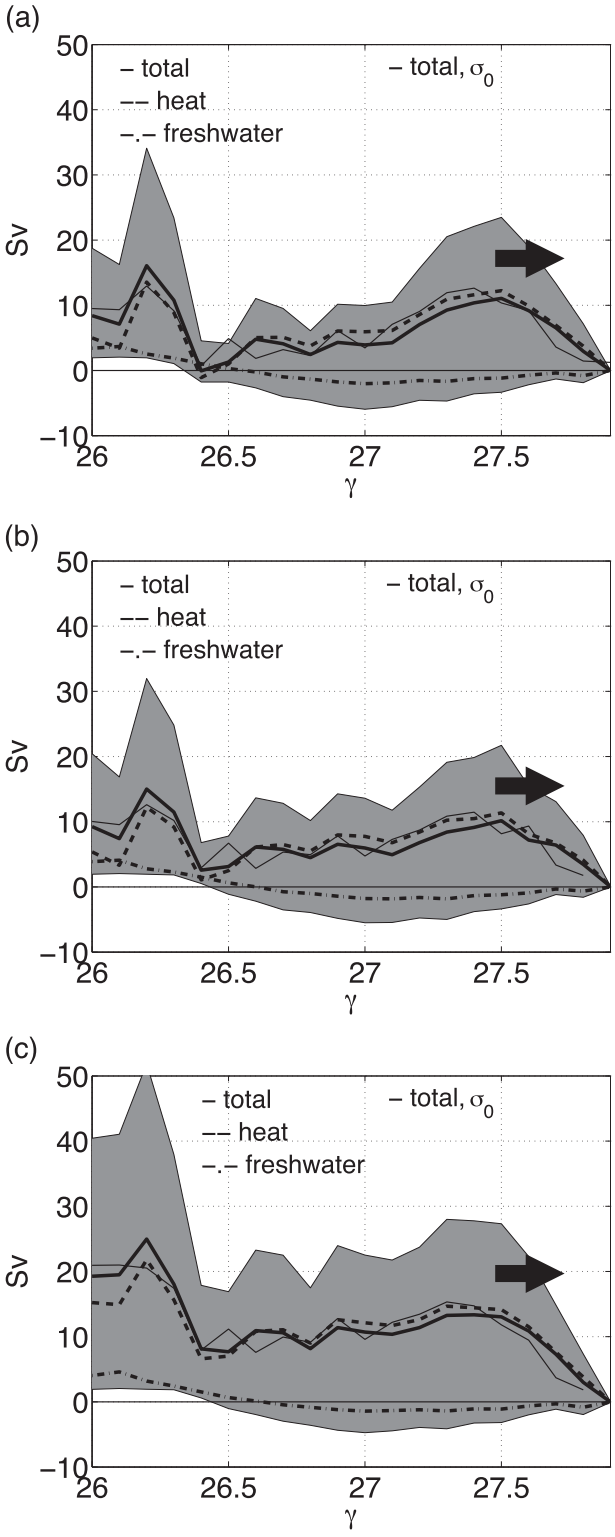

FIG. 6. Transformation rates (Sv) from air–sea fluxes for the North Atlantic basin from the (a) WHOI and (b) NOC climatologies and (c) the NCEP–NCAR reanalysis for the total (full line), and the air–sea heat flux (dashed line), and freshwater components (dot–dashed line). The thin continuous lines represent the total transformation rates calculated using potential density referenced to the sea surface σ_0; shading as in Fig. 3.

of dense waters by air–sea fluxes and diapycnal mixing in the Southern Ocean not resolved in our datasets, particularly problematic in the polar regions.

b. *Connections with the path of the Antarctic Circumpolar Current*

While the preceding water mass transformation analysis provides an integral view, the pattern of the air–sea fluxes and diapycnal mixing varies regionally and might connect to the path of the circulation. To assess this connection, the surface current speed in the ACC is diagnosed from the mean ocean dynamic topography data for the 1992–2002 period based upon data from surface drifters, satellite altimetry, surface winds, and the Gravity Recovery and Climate Experiment (GRACE) mission, provided at 0.5° resolution (Tapley et al. 2003; Maximenko and Niiler 2005).

The ACC is revealed by the strong surface, circumpolar flows, threading from the Argentine Basin, the Agulhas Current, south of New Zealand, and crossing the middle of the Indian and Pacific sectors of the Southern Ocean (Fig. 7a). The ACC deviates from a zonal trajectory principally through interactions with topography (Rintoul et al. 2001).

To aid comparison with the air–sea fluxes and diapycnal mixing responsible for the transformations, current data were interpolated onto the coarser grids, 2° × 7° resolution used for the surface fluxes and 6° × 7° resolution used for the Argo data, and averaged in neutral density bins with $\Delta\gamma = 0.1$. In neutral density coordinates, the ACC is directed eastward everywhere and reaches a maximum speed of $0.1\,\mathrm{m\,s^{-1}}$ at $\gamma = 26.8$ (Fig. 7b, full line). In comparison, there is an overall lightening from the equivalent heat fluxes reaching a maximum of $50\,\mathrm{W\,m^{-2}}$ at $\gamma = 27.3$ (Fig. 7b, dashed line), preferentially on the poleward side of the ACC maximum. The surface equivalent heat flux positively correlates with the surface current speed with a linear regression coefficient reaching $r = 0.8$ (Fig. 7c). The positive correlation is due to surface lightening occurring along the core of the ACC when the current is far from land (Figs. 7a,b). This surface lightening is consistent with an enhanced surface heating occurring as a result of the equatorward deflection of surface isotherms induced by the combined surface Ekman and eddy flow (Badin and Williams 2010).

Assessing the link between the vertical diffusivity and the current speed is handicapped by the lack of knowledge of the ACC structure at depth. To overcome this problem, the ACC is assumed to have an equivalent barotropic structure, such that the flow weakens with depth with a fixed *e*-folding scale but does not change direction (Killworth 1992; Gille 2003). At the sea surface,

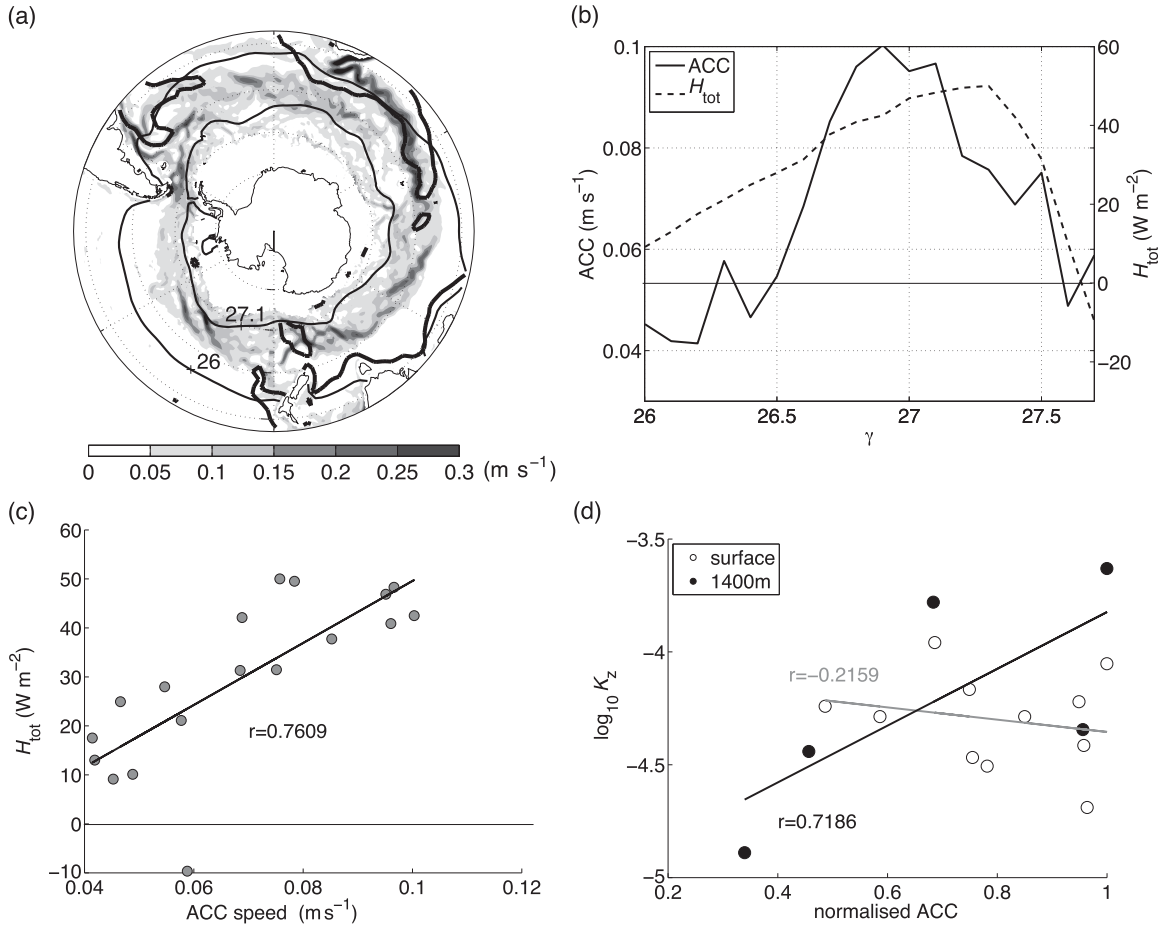

FIG. 7. (a) ACC surface speed (m s^{-1}) from 1992 to 2002 mean ocean dynamic topography with annual mean outcrops of $\gamma = 26$ and 27.1 surfaces (thick black lines) from the *World Ocean Atlas 2009*. (b) ACC surface speed (m s^{-1}, full line) and WHOI total equivalent heat fluxes (W m^{-2}, dashed line) averaged within neutral density bins $\Delta\gamma = 0.1$. Scatterplots for (c) $\mathcal{H}^*$ at the sea surface vs ACC speed (m s^{-1}) and (d) vertical diffusivity K_z at the sea surface (white dots) and at 1400-m depth (black dots) vs normalized ACC speed for each $\Delta\gamma = 0.1$ bin.

the vertical diffusivity does not correlate with the normalized ACC current speed (Fig. 7d, white dots). However, at 1400-m depth, the vertical diffusivity positively correlates with the normalized ACC current speed (Fig. 7d, black dots) with a linear regression coefficient reaching $r = 0.7$. This correlation suggests that there is an active role of strong currents in creating larger vertical diffusivity at depth.

This latter positive correlation between the ACC current speed and the vertical diffusivity is thought provoking. The energy sources for diapycnal mixing are likely to relate to the strength of the bottom flow of the ACC and the interaction with rough topography (Heywood et al. 2002; Naveira-Garabato et al. 2004; Wu et al. 2011). This flow interaction might generate lee waves, which then propagate upward and eventually break, possibly enhancing the diapycnal mixing at middepths (Nikurashin and Ferrari 2010).

5. Conclusions

The Southern Ocean plays a central role in forming mode waters and ventilating the global ocean, as well as in returning deep and bottom waters originally formed within the Southern Ocean or the North Atlantic to the sea surface. The Walin (1982) framework is applied here to understand how the water masses are transformed, for the first time in this region, exploiting in situ estimates of diapycnal mixing and combining with three different compilations of air–sea fluxes. While there are significant uncertainties in the air–sea fluxes, the estimates of diapycnal mixing and the data coverage over the Southern Ocean, the diagnostics provide a broadly consistent view of the effects of air–sea fluxes and interior diapycnal mixing. The air–sea fluxes and diapycnal mixing act on different water masses over the Southern Ocean, rather than locally compensate or

reinforce each other. Air–sea fluxes provide a transformation of intermediate waters to lighter mode waters, SAMW and AAIW, while diapycnal mixing leads to deep waters, UCDW and LCDW, becoming denser and bottom waters, AABW, becoming lighter. Air–sea fluxes are primarily responsible for the formation of lighter water masses in the Southern Ocean, while denser water masses are formed by a combination of unresolved surface heat, freshwater, and salt fluxes, augmented by diapycnal mixing in the Southern Ocean. The diapycnal mixing–induced lightening of bottom waters in the Southern Ocean is comparable to the air–sea flux-induced transformation of dense waters in the North Atlantic. Our data does not though adequately resolve the formation of denser bottom waters, formed through air–sea fluxes and ice interactions over the Antarctic shelves, as well as the diapycnal mixing–induced transformation over much of the Pacific sector.

While the water mass transformation provides an integral view, the air–sea fluxes and diapycnal mixing enabling this transformation vary with the strength of the ACC. The surface air–sea fluxes exhibit a positive correlation with the current speed with a general lightening along the core of the ACC when the current is far from land and in a zonal geometry. There is also enhanced diapycnal mixing at middepths in regions of stronger ACC flow, probably from the interaction of the bottom flow with rough topography.

Acknowledgments. GB was partially funded by DOE Grant DE-SC0005189 and NSF Grant AGS-1144302, and RGW by NER/T/S/2002/00439. We are grateful for the dynamic topography from N. Maximenko and P. Niiler, and for constructive feedback from S. Griffies and R. Toggweiler. We thank two anonymous referees for their constructive comments that strengthened the study.

REFERENCES

Antonov, J. I., and Coauthors, 2010: *Salinity.* Vol. 2, *World Ocean Atlas 2009,* NOAA Atlas NESDIS 69, 184 pp.

Badin, G., and R. G. Williams, 2010: On the buoyancy forcing and residual circulation in the Southern Ocean: The feedback from Ekman and eddy transfer. *J. Phys. Oceanogr.,* **40,** 295–310.

——, ——, and J. Sharples, 2010: Water-mass transformation in the shelf seas. *J. Mar. Res.,* **68,** 189–214.

Berry, D. I., and E. C. Kent, 2011: Air-sea fluxes from ICOADS: The construction of a new gridded dataset with uncertainty estimates. *Int. J. Climatol.,* **31,** 987–1001.

Cerovecki, I., L. D. Talley, and M. R. Mazloff, 2011: A comparison of Southern Ocean air–sea buoyancy flux from an ocean state estimate with five other products. *J. Climate,* **24,** 6283–6306.

——, ——, ——, and G. Maze, 2013: Subantarctic Mode Water formation, destruction, and export in the eddy-permitting Southern Ocean State Estimate. *J. Phys. Oceanogr.,* **43,** 1485–1511.

Downes, S. M., A. Gnanadesikan, S. M. Griffies, and J. L. Sarmiento, 2011: Water mass exchange in the Southern Ocean in coupled climate models. *J. Phys. Oceanogr.,* **41,** 1756–1771.

Gille, S. T., 2003: Float observations of the Southern Ocean. Part I: Estimating mean fields, bottom velocities, and topographic steering. *J. Phys. Oceanogr.,* **33,** 1167–1181.

Gregg, M. C., T. B. Sanford, and D. P. Winkel, 2003: Reduced mixing from the breaking of internal waves in equatorial ocean waters. *Nature,* **422,** 513–515.

Hanawa, K., and L. D. Talley, 2001: Mode waters. *Ocean Circulation and Climate,* G. Siedler, J. Church, and J. Gould, Eds., Academic Press, 373–386.

Heywood, K., A. C. Naveira-Garabato, and D. P. Stevens, 2002: High mixing rates in the abyssal Southern Ocean. *Nature,* **415,** 1011–1014.

Ito, T., and J. Marshall, 2008: Control of lower-limb overturning circulation in the Southern Ocean by diapycnal mixing and mesoscale eddy transfer. *J. Phys. Oceanogr.,* **38,** 2832–2845.

Iudicone, D., G. Madec, and T. J. McDougall, 2008: Water mass transformations in a neutral density framework and the key role of light penetration. *J. Phys. Oceanogr.,* **38,** 1357–1376.

Jackett, D. R., and T. J. McDougall, 1997: A neutral density variable for the world's oceans. *J. Phys. Oceanogr.,* **27,** 237–263.

Kalnay, E., and Coauthors, 1998: The NCEP/NCAR 40-Year Reanalysis Project. *Bull. Amer. Meteor. Soc.,* **77,** 437–470.

Killworth, P. D., 1992: An equivalent-barotropic mode in the fine-resolution Antarctic model. *J. Phys. Oceanogr.,* **22,** 1379–1387.

Klocker, A., and T. J. McDougall, 2010: Influence of the nonlinear equation of state on global estimates of dianeutral advection and diffusion. *J. Phys. Oceanogr.,* **40,** 1690–1709.

Kunze, E., E. Firing, J. M. Hummon, T. K. Chereskin, and A. M. Thurnherr, 2006: Global abyssal mixing inferred from lowered ADCP shear and CTD strain profiles. *J. Phys. Oceanogr.,* **36,** 1553–1576.

Locarnini, R. A., A. V. Mishonov, J. I. Antonov, T. P. Boyer, H. E. Garcia, O. K. Baranova, M. M. Zweng, and D. R. Johnson, 2010: *Temperature.* Vol. 1, *World Ocean Atlas 2009,* NOAA Atlas NESDIS 68, 184 pp.

Marsh, R., A. J. G. Nurser, A. P. Megann, and A. L. New, 2000: Water mass transformation in the Southern Ocean of a global isopycnal coordinate GCM. *J. Phys. Oceanogr.,* **30,** 1013–1045.

Marshall, D. P., 1997: Subduction of water masses in an eddying ocean. *J. Mar. Res.,* **55,** 201–222.

Marshall, J., and T. Radko, 2006: A model of the upper branch of the meridional overturning of the Southern Ocean. *Prog. Oceanogr.,* **70,** 331–345.

——, and K. Speer, 2012: Closure of the meridional overturning circulation through Southern Ocean upwelling. *Nat. Geosci.,* **5,** 171–180.

——, D. Jamous, and J. Nilsson, 1999: Reconciling thermodynamic and dynamic methods of computation of water mass transformation rates. *Deep-Sea Res. I,* **46,** 545–572.

Maximenko, N. A., and P. P. Niiler, 2005: Hybrid decade-mean global sea level with mesoscale resolution. *Recent Advances in Marine Science and Technology,* N. Saxena, Ed., PACON International, 55–59.

McCartney, M., 1977: Subantarctic Mode Water. *A Voyage of Discovery: George Deacon 70th Anniversary Volume,* M. V. Angel, Ed., Pergamon, 103–119.

McDougall, T. J., 1987a: Neutral surfaces. *J. Phys. Oceanogr.,* **17,** 1950–1964.

——, 1987b: Thermobaracity, cabbeling and water mass conversion. *J. Geophys. Res.,* **92** (C11), 5448–5464.

Naveira-Garabato, A. C., K. L. Polzin, B. A. King, K. J. Heywood, and M. Visbeck, 2004: Widespread intense turbulent mixing in the Southern Ocean. *Science,* **303,** 210–213.

Nikurashin, M., and R. Ferrari, 2010: Radiation and dissipation of internal waves generated by geostrophic motions impinging on small-scale topography: Application to the Southern Ocean. *J. Phys. Oceanogr.,* **40,** 1501–1519.

Nurser, A. J. G., R. Marsh, and R. G. Williams, 1999: Diagnosing water mass formation from air–sea fluxes and surface mixing. *J. Phys. Oceanogr.,* **29,** 1468–1487.

Osborn, T. R., 1980: Estimates of the local rate of vertical diffusion from dissipation measurements. *J. Phys. Oceanogr.,* **10,** 83–89.

Polzin, K. L., J. M. J. M. Toole, and R. W. Schmitt, 1995: Finescale parameterizations of turbulent mixing. *J. Phys. Oceanogr.,* **25,** 306–328.

Rintoul, S. R., C. Hughes, and D. Olbers, 2001: The Antarctic Circumpolar Current System. *Ocean Circulation and Climate,* G. Siedler, J. Church, and J. Gould, Eds., Academic Press, 271–302.

Sloyan, B., and S. R. Rintoul, 2001: The Southern Ocean limb of the global deep overturning circulation. *J. Phys. Oceanogr.,* **31,** 143–173.

Speer, K., S. R. Rintoul, and B. Sloyan, 2000: The diabatic Deacon cell. *J. Phys. Oceanogr.,* **30,** 3212–3222.

Suga, T., and L. D. Talley, 1995: Antarctic Intermediate Water circulation in the tropical and subtropical Atlantic. *J. Geophys. Res.,* **100,** 13 441–13 453.

Tapley, B. D., D. P. Chambers, S. Bettadpur, and J. C. Ries, 2003: Large scale ocean circulation from the GRACE GGM01 geoid. *Geophys. Res. Lett.,* **30,** 2163, doi:10.1029/2003GL018622.

Walin, G., 1982: On the relation between sea-surface heat flow and thermal circulation in the ocean. *Tellus,* **34,** 187–195.

Whalen, C. B., L. D. Talley, and J. A. MacKinnon, 2012: Spatial and temporal variability of global ocean mixing inferred from Argo profiles. *Geophys. Res. Lett.,* **39,** L18612, doi:10.1029/2012GL053196.

Williams, R. G., and M. Follows, 2011: *Ocean Dynamics and the Carbon Cycle: Principles and Mechanisms*. Cambridge University Press, 416 pp.

Wu, L., Z. Jing, S. Riser, and M. Visbeck, 2011: Seasonal and spatial variations of Southern Ocean diapycnal mixing from Argo profiling floats. *Nat. Geosci.,* **4,** 363–366.

Yu, L., X. Jin, and R. A. Weller, 2008: Multidecade global flux datasets from the objectively analyzed air–sea fluxes (OAFlux) project: Latent and sensible heat fluxes, ocean evaporation, and related surface meteorological variables. Woods Hole Oceanographic Institution Tech. Rep. OA 2008 01, 64 pp.

Zika, J. D., B. M. Sloyan, and T. J. McDougall, 2009: Diagnosing the Southern Ocean overturning from tracer fields. *J. Phys. Oceanogr.,* **39,** 2926–2940.